SAND2007-6573C

Electronically tunable plasmonic grating-gate terahertz detectors

E. A. Shaner, A. D. Grine, S.K. Lyo, J. L. Reno, and M. C. Wanke
Sandia National Laboratories, P.O. Box 5800, Albuquerque, NM 87185

S. J. Allen
Center for Terahertz Science & Technology, UC Santa Barbara, Santa Barbara, CA 93106

ABSTRACT

Split grating-gate field effect transistors (FETs) detectors made from high mobility quantum well two-dimensional electron gas material have been shown to exhibit greatly improved tunable resonant photoresponse compared to single grating-gate detectors due to the formation of a 'diode-like' element by the split-gate structure. These detectors are relatively large for FETs (1mm x 1mm area or larger) to match typical focused THz beam spot sizes. In the case where the focused THz spot size is smaller than the detector area, we have found evidence, through positional scanning of the detector element, that only a small portion of the detector is active. To further investigate this situation, detectors with the same overall length (1mm), but various widths, were fabricated and tested. The results indicate that indeed, only a small portion of the split grating gated FET is active. This finding opens up the possibility for further enhancement of detector sensitivity by increasing the active area.

Keywords: Field effect transistors, high mobility, two-dimensional plasmons, terahertz, focal plane arrays, bolometers

1. INTRODUCTION

Plasmons (charge oscillations), in semiconductors present resonances that can be engineered both by geometry and carrier density control. For detection in the terahertz regime, two-dimensional (2D) plasmons in FET structures are under investigation using various geometries[1-6]. Due to the significant wavevector mismatch between typical semiconductor 2D plasmons and free space radiation, in general, coupling needs to be facilitated by some aspect of the device geometry. In grating-gate detectors, the FET gate serves this purpose by modulating both the carrier density in the channel and the incident radiation in order to allow excitation of 2D plasmons. While this was first demonstrated nearly three decades ago in silicon inversion layers[7], work is still under way to develop devices based on 2D plasmon excitations as fast, sensitive, tunable, photodetectors. A significant step towards this end was the development of the split grating-gate detector which increased the responsivity by 3 orders of magnitude[8], to several V/W, compared to the FETs having only a single grating-gate. While this was a significant improvement, the noise equivalent power (NEP) of these detectors is 10^{-7}W/√Hz. For these detectors to ultimately be useful, this figure of merit needs to be improved by at lease 2-3 orders of magnitude. Along these lines, this paper details recent findings which provide evidence that the active area of the split grating-gate detector is in fact relatively small compared to the overall detector size, opening up the possibility of much further improvement.

2. BACKGROUND

Typical carrier densities in AlGaAs/GaAs quantum well systems (~10^{11}cm^{-2}) require gratings with periods of several microns in order to couple THz radiation (several hundred microns wavelength) to 2D plasmons in the channel. The dispersion relation for plasmons in 2D is given approximately by[9]:

$$f_p^2 \propto n(V_G)k_j \,. \quad \text{Eq. 1}$$

Here f_p is the plasmon resonant frequency, $n(V_G)$ is the gate controlled carrier density, $k_j = jk_1$ is the j^{th} harmonic mode (j = 1, 2, 3,...) and $k_1=2\pi/a$, where a is the grating period.

To date, we have shown that 2D plasmons in both single and double quantum well high mobility material can be coupled to THz radiation by a grating gate[2]. In the case of single quantum well material, the carrier density involved in determining the plasmon resonance condition is simply the channel density underneath the grating gate fingers[3]. In the double quantum well case, while it is not obvious, we have found that the density of the two layers can simply be added and considered approximately as a single quantum well having the combined carrier density[2]. In the specific case of a single quantum well split grating-gate detector, we have shown that a single detector with a 4μm period can have a resonant photoresponse tunable from 600GHz to 1THz by varying only the carrier density in the channel through application of a gate bias[8].

3. EVIDENCE OF SMALL ACTIVE AREA

Figure 1 shows the split grating-gate detector that provided the initial evidence of a small detector active area. The detector was fabricated from a single modulation-doped GaAs-AlGaAs quantum well, 40 nm wide, formed 200 nm below the wafer surface. The QW has approximate electron density of 2.5 x10^{11}cm^{-2} and mobility $\mu \approx 5 \times 10^6 cm^2/V \cdot s$. The device was fabricated on an isolation mesa etched completely though the QW. Standard annealed Ohmic contacts form the source and drain. The grating gate, split into 3 sections, is comprised of 20 nm Ti/50 nm Au and has a 4 μm, 50% duty cycle period over a 2 mm x 2 mm area. The gate sections, labeled in Fig. 1, are a large area gate on the source side of the detector (V_{GS}), a single gate line bisecting the device (V_{FG}) and another large area gate on the drain side of the detector (V_{GD}).

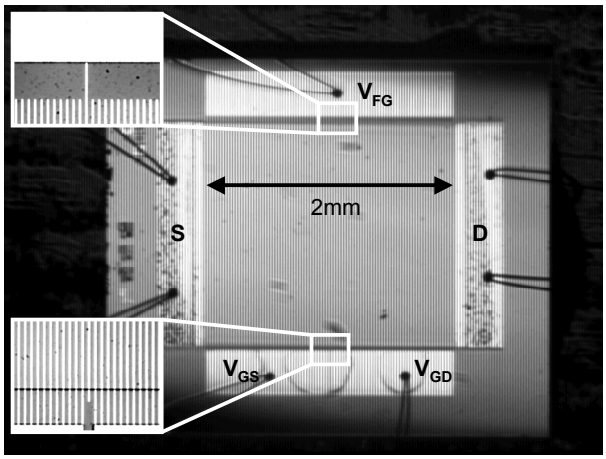

Fig. 1: Split gate detector with 2mm x 2mm grating gate area. Period of grating is 4μm, grating lines are 2μm wide. Zoomed regions show the detail of the split gate structure.

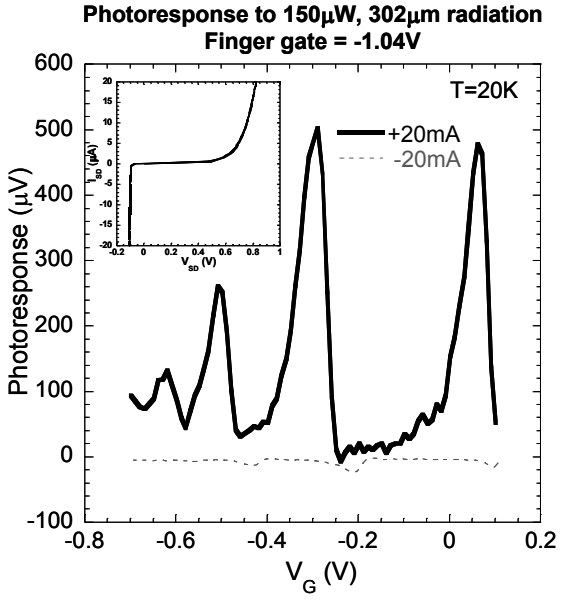

Fig. 2: 1THz photoresponse as a function of gate voltage. Inset shows the IV characteristics of the split grating-gate detector when the tuning gate bias is 0V and the finger gate bias is -1.04V. The main plot shows the resonant photoresponse to 1THz as tuning gate bias, V_G, is swept.

To measure photoresponse, the sample is mounted on the cold finger of a continuous flow cryostat. The pinchoff voltage (where full depletion occurs) was approximately -0.75V for the material from which the detector of Fig. 1 was made. The inset of Fig. 2 shows the IV characteristics of this detector when V_{FG} = -1.04V, about 300mV past the pinchoff voltage, with V_{GS} tied to the source contact and V_{GD} tied to the drain contact (so zero effective bias on the source and drain side channels) at T=20K. Under these conditions, one can see the detector exhibits diode like characteristics due to the barrier formed between source and drain. While the photoresponse mechanisms related to this barrier are still under investigation, it is thought that the quadrant of positive current/voltage (from source to drain) yields a bolometric photoresponse while the negative current/voltage quadrant may be rectification. For measurements, the sample is illuminated, using f2 focusing optics, by a CO2 pumped far-infrared laser operating on the lines of formic acid. The response to 302μm radiation (~1THz) is shown in Fig. 2 with V_{FG} = -1.04V. An adding circuit is used to feedback the source drain voltage, V_{SD}, to the large gate on the source side of the single finger. This is done to create the condition that $V_{GS}=V_{GD}=V_G$, the tuning gate

voltage. As V_G is swept, the portions of the channel under the grating gate lines are depleted, reducing the carrier density. When the conditions of Eq.1 are met, we get resonant plasmon peaks in the photoresponse.

With f2 optics, and a 1THz laser line, a diffraction limited spot size of about 1.5mm is expected. Since this is smaller than the detector area, such a configuration can be used to roughly map out the active area of the detector by moving the detector in the focal plane and measuring the photoresponse. In every split grating-gate detector to date, we have observed that, when operating under the conditions of the IV in Fig.2, in the negative current/voltage quadrant, only the gate on the source side of the device provides a tunable response, and in the positive current/voltage quadrant, only the drain side provides the response. The initial motivation for imaging the active area was to investigate these effects.

Figure 3a shows the beam image, as a filled contour plot, when the split grating-gate detector is biased to I_{SD} = 20μA, V_{SD} = 0.8V, V_G = -0.3V, V_{FG} = -1.04V. This is the same set of conditions as shown for the +20μA photoresponse of Fig. 2, with V_G set to sit on a large resonant peak. In this setup, the detector was positioned so that the grating lines ran along the x direction (imagine the device in Fig. 1 rotated 90 degrees), while the electric field of the laser is polarized in the y-direction. The shape of the spot was verified independently, by using a THz beam profiler, to be Gaussian. However, as seen in Fig. 3a, the image is asymmetric. Along the x-direction, the beam seems to map out the 2mm 'height' of the detector, while along the y-direction, it is clear that something less than the 2mm width of the detector is responding to the radiation.

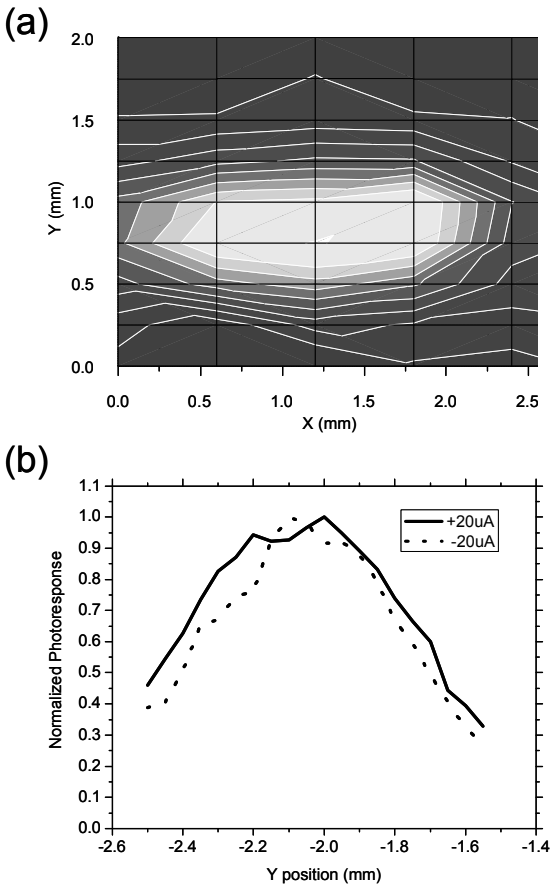

Fig. 3: Results of 1THz beam imaging. (a) VFG = -1.04V, ISD=+20uA, Vg=-0.3V. detector scanned in X and Y. Grating lines run along the X direction. In the X direction, the 2mm size of the detector is clearly mapped out. In the Y direction, it is apparent that less than 2mm of the detector is active leading to the asymmetric image. (b) Higher resolution scans (on resonance) in the y-direction only using both positive current and negative current operating points.

To investigate the active region further, higher resolution position scans in the y-direction were performed while the detector was biased (see Fig. 2) onto the positive current/voltage resonant peak at V_G= -0.3V, and the negative current/voltage resonant peak at V_G=-0.21V respectively. The results are shown in Fig. 3b. While we expected to see a significant shift in the active area between the drain side (positive quadrant, solid trace) and source side (negative quadrant, dashed trace), it appears that the scans are nominally unchanged. One plausible explanation is that only a very small region, near the single finger gate line that bisects the device, contributes to the observed photoresponse.

4. REDUCTION OF DEVICE WIDTH AND NUMBER OF GRATING LINES

To investigate the active area more thoroughly, split grating-gate detectors were fabricated with identical grating parameters, 4μm period, 50% duty cycle, 1mm height, but with varying widths of 1mm (250 grating lines), 400μm (100 grating lines, and 80μm (20 grating lines). All detectors were made on the same piece of high-quality QW material in the same processing run so as to reduce any fabrication errors. The detectors are pictured in Fig. 4 along with zoomed

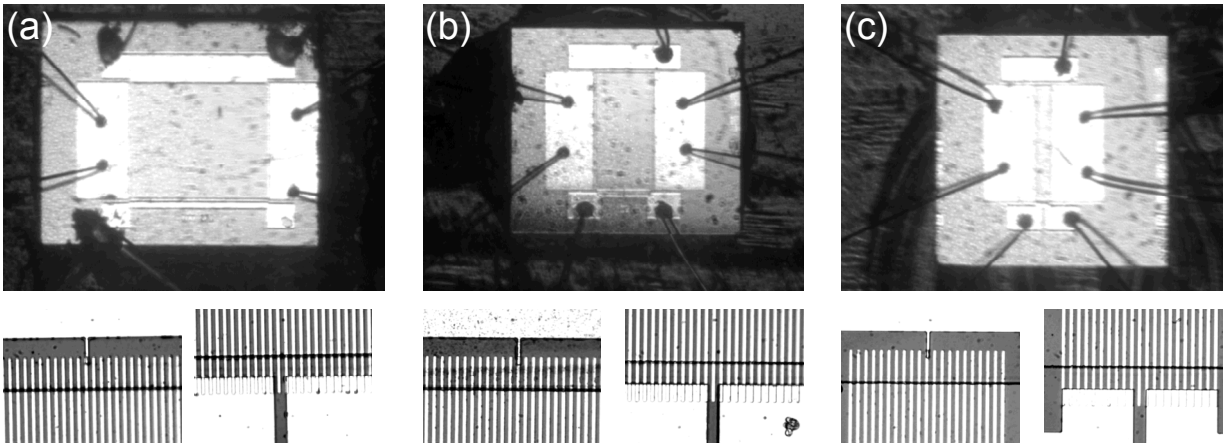

Fig. 4: Detectors used to determine the width dependence on the photoresponse. (a) 1mm x 1mm grating, 125 lines on each side of the finger gate. (b) 1mm x 400μm grating, 50 lines on each side of the finger gate. (c) 1mm x 80μm grating, 10 lines on each side of the finger gate. All images were taken using the same magnification to provide a sense of scale. Below each main image are zoomed images of the finger gate (left) and tuning gate (right) connections. Note that in the case of the 80μm wide detector (c) the entire grating fits in the zoomed field of view.

views of the gate detail below each detector. All bonding pads on the detectors are identical. The source/drain pads are 1mm x 400μm where as the gate connection pads were all of the same vertical dimensions, but varied in width to accommodate the variation in the number of gate lines per device.

Photoresponse measurements were performed, at T=20K, on the three detectors in the manner already described. The main difference in this case was that the illumination frequency was 694GHz instead of 1THz. The beam spot size in this case is now approximately 2.2mm, larger than all detectors in this experiment. For all measurements, the incident power, measured with a Thomas Keating power meter, was approximately 1mW.

The photoresponse for the 3 different size detectors is displayed in Fig. 5. While there are some clear differences between the measured spectra vs. the tuning gate bias V_G, the main point is clear; the number of grating lines on either side of the single finger gate, does not matter a great deal. Looking in particular at the photoresponse near V_G=0V, it only ranges between 2700uV and 3200uV from detector to detector.

The detector geometries displayed in Fig. 4 have been fabricated from other high mobility single quantum well material. In all cases, we have observed the same trend displayed in Fig. 5. The conclusion drawn here is that, in order to make a more sensitive grating-gate detector, a way must be found to increase the active area of the device so that more of the grating can contribute to the overall photoresponse. While it is plausible that the bonding pads and wires create antennas that couple radiation into the detector, we have not investigated those effects to date. It is possible to fabricate 'center-fed' devices, as will be shown in the next section, which can remove this possibility, however, those devices with

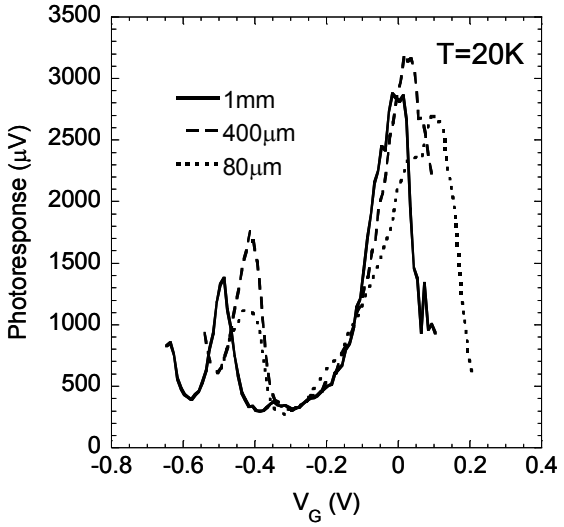

Fig. 5: Response of detectors of varying width, but identical grating parameters, to 694GHz illumination when operating on a positive current/voltage split-gate operating point.

varying grating widths have not been made at this time. We do note that the results displayed in Fig. 3b for a 2mm x 2mm grating do appear to show that bond pads and wires do not act as antennas, however, as the device dimensions are reduced, this may not be the case.

5. SPLIT GRATING-GATE DETECTORS ON THERMALLY ISOLATING MEMBRANES

As alluded to earlier, the operating quadrant of positive current/voltage in split gate operation is thought to provide a bolometric response mechanism. One approach to both verify this mechanism and increase the active area of the devices, is to fabricate the split grating-gate detector on a thermally isolating membrane[10].

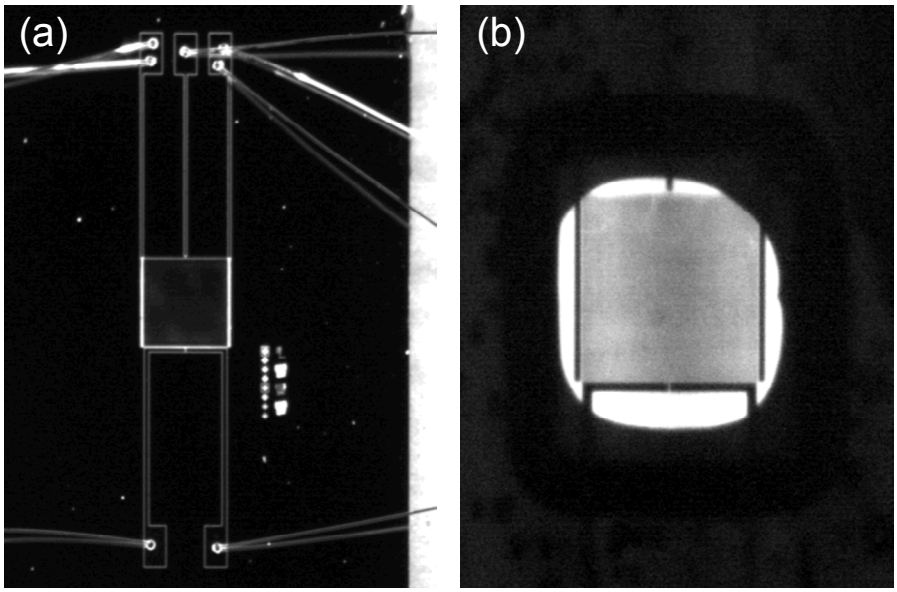

Fig. 6: Split grating-gate detectors made from double quantum well material. (a) The control device made on a thick substrate. Grating lines (not visible) run in the vertical direction. The contact pads for this device are several mm away from the detector which both eliminates antenna effects and allows for membrane isplation of the detector element. (b) The 'membrane' detector with backside illumination used to emphasize the area which has been eched out from behind the detector.

Devices were fabricated from from modulation-doped GaAs–AlGaAs double quantum wells (DQWs). The wells are separated by 70 Å and are each 200 Å wide. The DQW has a combined electron density of 4.14×10^{11} cm^{-2} and low temperature mobility $1 \times 10^6 cm^2/Vs$ determined from Hall measurements. Two detectors of identical geometry (center fed 1mm x 1mm grating, Fig. 6a) were made from this material. To isolate one of the detectors on a membrane, a backside aligner was used to pattern a square in photoresist on the backside of the chip. Then, a mixture of H_2SO_4:H_2O_2 (1:4) was used to remove approximately 550microns of substrate material. The sample was finished off using Citric Acid(1gm/mL):H_2O_2 (4:1) that etched to an AlGaAs etch stop layer beneath the DQWs. The resulting membrane is approximately 4μm thick. Figure 6b shows the membrane detector with backside IR illumination to emphasize the area that was etched from beneath the detector.

As was the case in Sec. 3 & 4, the single finger gate in the split-gate structure was biased beyond pinchoff to create IV characterstics similar to that of the inset to Fig. 2. Photoresponse measurements were made in the quadrant of positive current/voltage under illumination by a 694GHz laser focused with f2 optics. Figure 7 shows the rather remarkable difference in responsivity between the two detectors. In Fig. 7a, a maximum resonant response (V_G=-0.95V) of only 120μV to 750μW is found for the thick detector while in Fig. 7b, approximately 500μV photoresponse (subtracting 100μV background at VG=-1.27V) was found with only 70μW power. The membrane detector therefore exhibits ~50X

responsivity improvement over its thick counterpart. We have performed this experiment on several matched sets of detectors and obtained the same results every time.

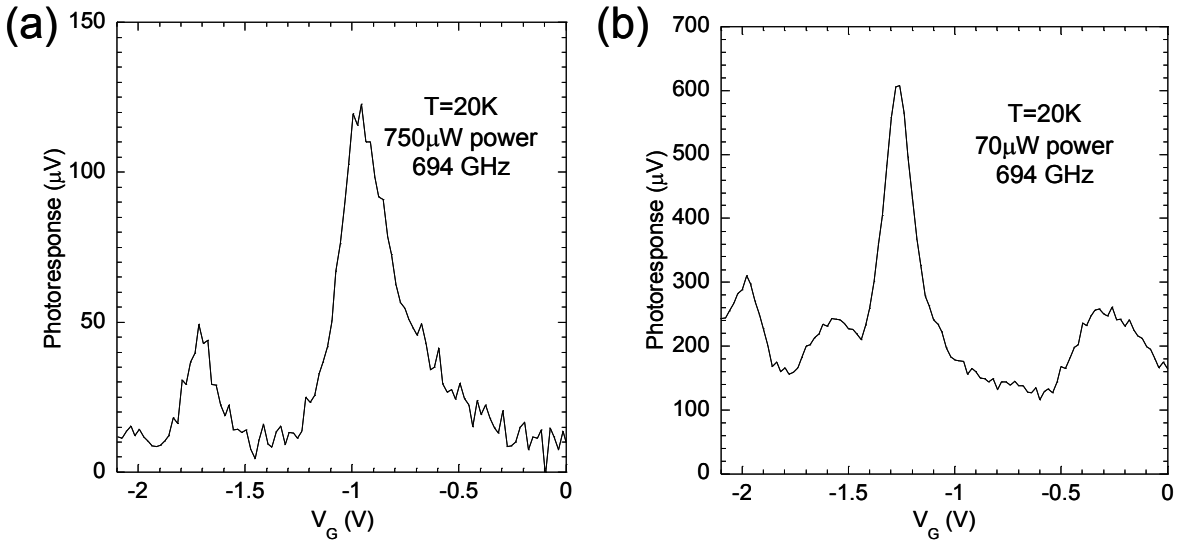

Fig. 7: Photoresponse of 'thick' and 'membrane' detectors. (a) The photoresponse of the 'thick' detector to 750μW of 694GHz radiation. (b) The photoresponse of the 'membrane' detector to only 70μW of 694GHz radiation. The corresponding responsivity increased by a factor of ~50.

To further understand the improvement in photoresponse introduced by membrane isolation, the thermal transport in the detectors was modeled. As shown in Fig. 8a, the thick detector was modeled as a 1 mm diameter, 600 μm tall cylinder with the detector on the top surface and the bottom held at T=20 K. The membrane detector, Fig. 8b, was modeled as a 4μm thick disk with its boundary held at T=20K. When considering uniform absorption of power on the detector surface, the center of the thin disk was calculated to have a differential temperature approximately 40 times higher than that of the center of the top of the cylinder. This prediction agrees reasonably well with the factor of 50 improvement observed in photoresponse.

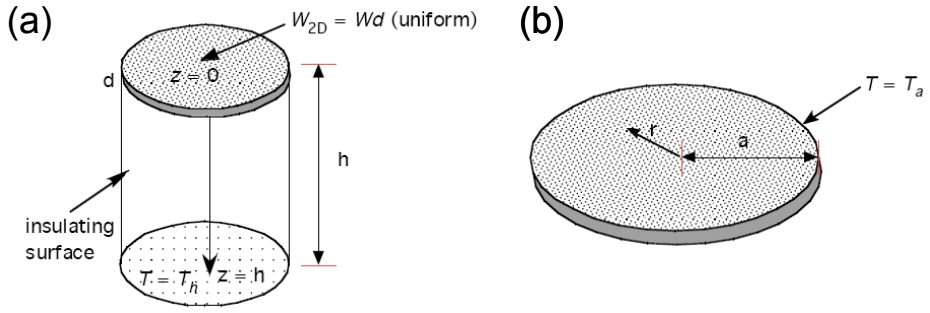

Fig. 8: Model used to simulate thick and membrane detector thermal transport. (a) Thick detector: Insulating cylinder with h=600μm, 1mm diameter, bottom of cylinder held at base temperature. (b) Membrane detector: Disk with diameter of 1mm, thickness 4μm, boundary held at base temperature.

6. CONCLUSIONS

While the split grating-gate detector has shown great improvement relative to its single-gate predecessors, the noise-equivalent power (NEP) is currently around 10^{-7}W/√Hz. By illuminating large split grating-gate detectors with THz radiation having a focused spot size smaller than the detector, we have found that the entire detector is not contributing

to the photoresponse. By fabricating detectors of varying widths, we have in fact found that the grating area can be shrunk by over 90%, and we still observe the same magnitude of resonant photoresponse. In an attempt to increase the active area of the detector, we have fabricated split grating-gate detectors on thermally isolating membranes. This led to an improvement by a factor of 50 in the resonant photoresponse. While there is a great deal of ground left to cover before these detectors can truly compete with Schottky diode detectors ($\sim 10^{-10}$W/$\sqrt{\text{Hz}}$) in terms of NEP, these findings show that there are paths forward which may lead to this desired level of performance.

The authors would like to thank Greg Aizin (CUNY) for helpful discussions. Sandia is a multiprogram laboratory operated by Sandia Corporation, a Lockheed Martin Company, for the United States Department of Energy's National Nuclear Security Administration under contract DE-AC04-94AL85000. Work at UCSB was supported by an ARO-DURINT - The Science and Technology of Nano/Molecular Electronics: Theory, Simulation and Experiment and continues under the University at Buffalo NSF NIRT THz Collaboratory: ECS0609146.

[1] E. Batke, J. Kaminsky, J. P. Kotthaus, and J. Spector "Tunable far-infrared photovoltaic response in semiconductor field-effect devices". *Appl. Phys. Lett.* **54**, 131-133 (1989).

[2] X. G. Peralta, S. J. Allen, M. C. Wanke, N. E. Harff, J. A. Simmons, M. P. Lilly, J. L. Reno, P. J. Burke, and J. P. Eisenstein "Terahertz photoconductivity and plasmon modes in double-quantum-well field-effect transistors". *Appl. Phys. Lett.* **81**, 1627-1629 (2002).

[3] E. A. Shaner, M. Lee, M. C. Wanke, A. D. Grine, J. L. Reno, and S. J. Allen "Single-quantum-well grating-gated terahertz plasmon detectors". *Appl. Phys. Lett.* **87**, 193507 (2005).

[4] A. El Fatimy, S. B. Tombet, F. Teppe, W. Knap, D. B. Veksler, S. Rumyantsev, M. S. Shur, N. Pala, R. Gaska, Q. Fareed, X. Hu, D. Seliuta, G. Valusis, C. Gaquiere, D. Theron, and A. Cappy "Terahertz detection by GaN/AlGaN transistors". *Electron. Lett* **42**, 1342-1344 (2006).

[5] E. A. Shaner, M. C. Wanke, M. Lee, J. L. Reno, S. J. Allen, and X. G. Peralta, "Grating gated FET's as narrowband, tunable terahertz detectors" in *Terahertz for Military and Security Applications III*, edited by R. J. Hwu, D. L. Woolard, and M. J. Rosker, Vol. 5790, pp. 116-122, SPIE, Bellingham, 2005

[6] E. A. Shaner, M. Lee, M. C. Wanke, A. D. Grine, J. L. Reno, and S. J. Allen, "Tunable THz detector based on a grating gated field-effect transistor" in *Terahertz and Gigahertz Electronics and Photonics V*, edited by R. J. Hwu and K. J. Linden, Vol. 6120, pp. 612006, SPIE, Bellingham, 2006

[7] S. J. Allen, D. C. Tsui, and R. A. Logan "Observation of 2-dimensional plasmon in silicon inversion layers". *Phys. Rev. Lett.* **38**, 980-983 (1977).

[8] E. A. Shaner, A. D. Grine, M. C. Wanke, M. Lee, J. L. Reno, and S. J. Allen "Far-infrared spectrum analysis using plasmon modes in a quantum-well transistor". *IEEE Phot. Tech. Lett.* **18**, 1925-1927 (2006).

[9] Tsuneya Ando, Alan B. Fowler, and Frank Stern "Electronic properties of two-dimensional systems". *Rev. Mod. Phys.* **54**, 437 (1982).

[10] E. A. Shaner, M. C. Wanke, A. D. Grine, S. K. Lyo, J. L. Reno, and S. J. Allen "Enhanced responsivity in membrane isolated split-grating-gate plasmonic terahertz detectors". *Appl. Phys. Lett.* **90**, 181127 (2007).